Materials and Structures (2015) 48:1803–1813
DOI 10.1617/s11527-014-0273-z

ORIGINAL ARTICLE

High strain rate behaviour in tension of steel B500A reinforcing bar

Ezio Cadoni · Matteo Dotta · Daniele Forni · Nicoletta Tesio

Received: 10 June 2013 / Accepted: 27 February 2014 / Published online: 4 March 2014

Abstract In reinforced concrete structures under severe dynamic loading, as impact and blast, both concrete and reinforcing bars are subjected to high strain-rates. While the dynamic tensile behaviour of concrete is the subject of many researches, the behaviour of the reinforcing steel under high strain rate has been not completely considered yet. Such behaviour is of capital importance in the structural assessment under the abovementioned loading conditions. This is the reason why an experimental program on rebar, stirrup and wire steels under high strain rate in tension is running at the DynaMat Laboratory. In this study the effect of high strain rate on the mechanical properties of B500A steel reinforcing bars in tension has been analysed. The steel of three different bars having diameter of 6, 8 and 10 mm have been investigated. The experiments have been carried out by means of a Split Hopkinson Tensile Bar at 250, 500 and 1000 s^{-1}. Finally the parameters of the well-known Johnson–Cook and Cowper–Symonds materials models have been obtained.

Keywords High strain rate · Reinforcing bar · B500A · Split Hopkinson Tensile Bar · Constitutive material model

E. Cadoni (✉) · M. Dotta · D. Forni · N. Tesio
DynaMat Laboratory, University of Applied Sciences of Southern Switzerland, 6952 Canobbio, Switzerland
e-mail: ezio.cadoni@supsi.ch

1 Introduction

The study of the response of reinforced concrete (RC) structures under transient dynamic loading for many years has been limited to very specialized fields in both military and civilian applications (protective structures or nuclear power plants). Recent events, due to natural or man-made causes, have highlighted the vulnerability of RC structures to those dynamic loads as impact and blast. In the last decades particular attention has been addressed to socially-sensitive structures, such as for example tunnels, sheltering structures, nuclear power plants, high-rise buildings, bridges and off-shore platforms. For most of these buildings has been required an assessment taking into account their vulnerability, or their potential to mitigate severe dynamic loads, such as impacts or blasts due to terroristic attack.

Thus nowadays the comprehension of the mechanical behaviour of RC structures under high dynamic loadings is consequently became of extreme importance [1].

Asprone et al. [2, 3] had shown in the evaluation of the structural behaviour of critical infrastructures as a bridge under severe dynamic load conditions, characterized by high intensity and short duration, the role played by the dynamic properties of materials is fundamental.

Till now experimental campaigns on the dynamic behaviour of reinforcing steel are rare, as a consequence still remain a lack of satisfactory data. This is

the reason why an experimental program on rebar, stirrup and wire steels under high strain rate in tension is running at the DynaMat Laboratory of the University of Applied Sciences of Southern Switzerland.

The effects of increasing strain rate on mechanical properties of steel, used for reinforcing bar, can be described as an enhancement of the yield strength (f_y), ultimate tensile strength (f_t) and uniform strain. Experimental evidence shows that the elastic modulus generally remains insensitive to the strain rate. Often, when the strain rate is very high, the dynamic yield strength may increase beyond that of the ultimate strength [4–6]. Dowling and Harding [7] tested mild steel in tension, in the strain rate range of $10^{-3} \div 2 \times 10^{-3}$ s^{-1}, using for higher strain rate a tensile version of Split Hopkinson Pressure Bar (SHPB). They found that mild steel, being a material with body-centred cubic structure, is affected by a strong strain rate sensitivity. In these experiments were found that the lower yield strength can almost be doubled while the ultimate tensile strength can be increased by about 50 %. Moreover, the upper yield strength was considerably higher and the failure strain decreases with increasing strain rate.

Increasing the strain rate the increment of the dynamic ultimate tensile strength is slightly less than those of the dynamic yield strength at the same rate.

Malvar [8], conducted a literature review by considering the strain rate effect on the properties of reinforcing bars with yield stress ranging from 290 to 710 MPa, in the strain rates range $10^{-4} \leq \dot{\varepsilon} \leq 10$ s^{-1}. Three different groups of reinforcing bar steel were analysed with yield stress of 275, 413 and 517 MPa. From this analysis a formulation to evaluate the dynamic increase factor (DIF), ratio between dynamic and static value, of the reinforcing bar with the increasing of strain rate was proposed. Unfortunately higher strain rate were not considered and it is well known that blast pressures normally produce loads associated with strain rates that can reach 10^2–10^3 s^{-1}.

Other past [9, 10] and recent [3, 6, 11–14] researches confirmed the mechanical structural steel improvement of both yield and ultimate tensile strength as well as the fracture strain at high strain rates.

The CEB bulletin [15] and more recently the Model Code 2010 [16] described the strength enhancement of steel reinforcing bars in terms of DIF. DIF formulations are widely used to calibrate numerical model for the evaluation of RC structures submitted to high strain rates expected for seismic, impact and blast loadings [17].

As far as we know no previous researches are focused on the high strain rate behaviour of cold drawn rebar mainly used in Civil Engineering as welded wire mesh (known also as welded wire fabric) and stirrups.

The cold drawn is a process in which the cross sectional area of wire, bar or tube is reduced by drawing the material through a die without any pre-heating. It is well known that this process changes the mechanical properties of the steel: due to the forced section reducing, both an high hardening and strengthening increase as well as a reduction in ductility were obtained.

Welded wire mesh is a prefabricated reinforcement consisting of deformed or smooth wires welded together in square or rectangular grids. This type of reinforcement, where relatively regular reinforcement are possible, is widely used in both precast and on-site concrete constructions, such as for example walls, bridge decks, slabs and as shear reinforcement in RC elements. The main benefits in using these elements are time and financial saving as well as the easy on-fabric quality control. Cold drawn rebar are also widely used as surface ground support in mining applications [18].

The material object of this research is a commercial B500A steel, manufactured through a cold-forming process of wire rod and available as coils or bars in a range of 5–12 mm in diameter.

The purpose of this article is to both highlight the strain-rate sensitiveness and to quantify the strength enhancement in terms of the DIF of the B500A steel in a wide range of strain rates (10^{-4}–10^3 s^{-1}) by analysing specimens turned from three different bars with 6, 8 and 10 mm in diameter, respectively.

Finally, the parameters of the Johnson–Cook and Cowper–Symonds materials models have been obtained.

2 Material

The B500A grade is a commercial high-strength reinforcing steel produced by cold forming process available in diameter ranging from 5 to 12 mm in coils or bars. This quality of steel is mostly used as transversal reinforcing, like stirrups, or for the production of welded wire meshes.

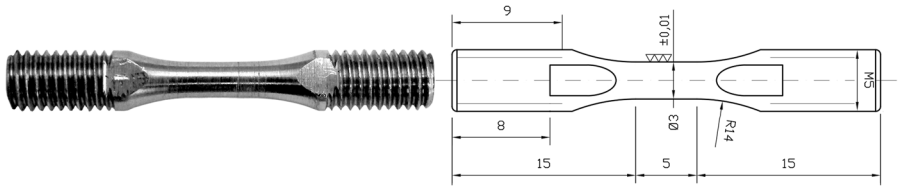

Fig. 1 Sample geometry

Table 1 Materials composition

Bars	C	S	Cr	Ni	Mn	Si	V	Fe
$d = 6$ mm	0.19	0.020	0.23	0.10	0.44	0.18	–	Balanced
$d = 8$ mm	0.18	0.030	0.17	0.10	0.48	0.18	–	Balanced
$d = 10$ mm	0.17	0.010	0.03	0.02	0.46	0.18	–	Balanced

The capital letter B, preceding the nominal yield strength (500 MPa), designates reinforcing steel, while *A* is the ductility class in accordance with EN 1992-1-1 [19] who defines in terms of the ratio f_t/f_y three ductility classes:

A (low ductility: $f_t/f_y \geq 1.05$), *B* (normal ductility: $f_t/f_y \geq 1.08$) and *C* (high ductility: $1.15 \leq f_t/f_y \leq 1.35$).

The grade B500A steel is conform to both the Swiss [20] and French standards [21], as well other European countries.

Three different diameters 6, 8 and 10 mm of this reinforcing steel were used. The specimens were obtained by turning these three bars, obtaining the common geometry, 3 mm in diameter and 5 mm of gauge length (Fig. 1), used in dynamic testing with the Split Hopkinson Tensile Bar, SHTB [22].

The chemical composition of the three bars were obtained by inductively coupled plasma/optical emission spectrometry and carbon and sulphur analyser, the results are reported in Table 1. To compare the microstructure of the B500A steel two specimens of 6 and 8 mm in diameter were prepared for optical microscopy using standard laboratory techniques for grinding and polishing. Micrographs shown in Fig. 2 confirm that the two bars have the same microstructure. It is possible to observe how the bar with lower diameter has a well distributed granulometry than to the larger one due to the cold-drawn procedures. The turning process adopted to prepare the specimen has been conducted at low velocity taking care to lubricate in order not to induce high temperature on the specimen. The materials subjected to this turning process do not change their mechanical characteristics neither the microstructures. In the border of the specimen the microstructure could be slightly modified but the extension of this zona is limited to few microns, that is three order of magnitude less respect to the diameter of the specimen so its effect can be neglected.

3 Experimental procedures

It is well known that the cold forming process changes the mechanical properties of the steel. The forced section reducing, necessary in order to obtain small diameter, produce both an high hardening and strengthening increase as well as a reduction in ductility. With the purpose of studying this phenomena, three different diameter were analysed, 6, 8 and 10 mm.

Different set-ups were used for the tensile mechanical characterisation at room temperature. The target strain rates were set at the following four levels: 10^{-4}, 250, 500 and 1000 s^{-1}.

Quasi-static tests were carried out by means of a universal electromechanical machine Zwick/Roell, while dynamic test were performed at high strain rates by means of a SHTB [13, 14, 22–25] installed at the DynaMat Laboratory (Fig. 2). Additionally some tests at intermediate strain rate were carried out using a Hydro-Pneumatic Machine described in [23].

SHPB consists of two cylindrical high strength steel bars, having a diameter of 10 mm, with a length of

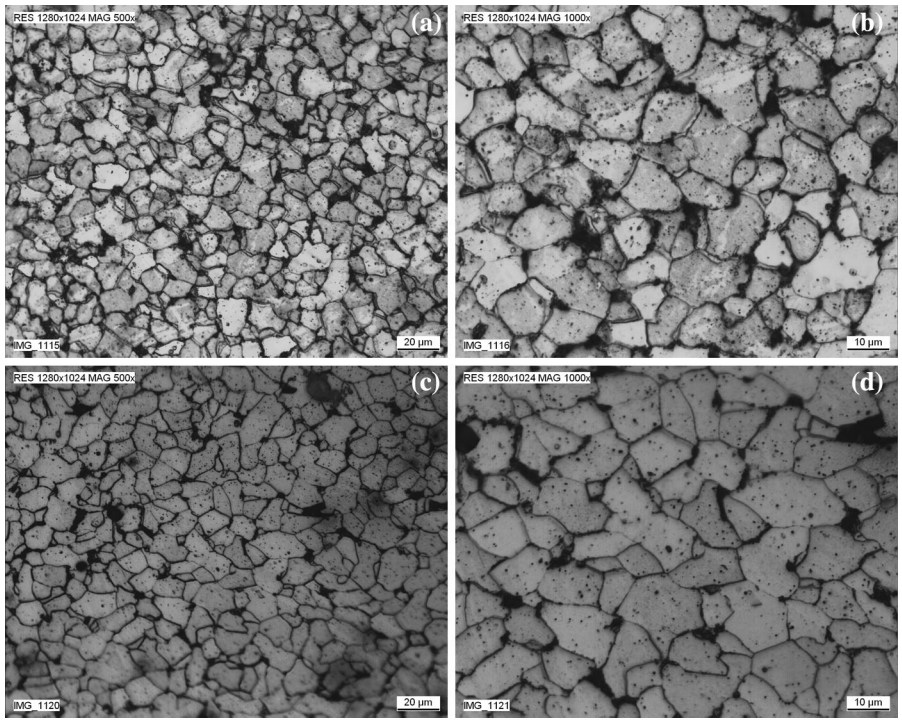

Fig. 2 Micrographs of B500A steel: **a**, **b** 6 mm diameter and **c**, **d** 8 mm diameter

respectively 9 and 6 m for the input and the output bar, respectively. Part of the first bar is used a pre-tension bar while the rest is used as input bar (Fig. 3).

In order to measure incident, reflected and transmitted pulses acting on the specimen screwed between the two bars, both input and output bars have been instrumented with strain gauges placed at 800 mm from the specimen.

The present set-up has the following two conditions, the bar diameter (10 mm) is smaller in comparison with the pulse length (12 m), and the specimen length is short so that the time taken by the wave to propagate through the specimen is short compared to the total time of the test. These conditions allow many reflections inside the specimen necessary for reaching a homogeneous stress and strain distribution along the specimen gauge length, what means also equilibrium of the forces acting on both ends of the specimen [6].

Being the two bars elastically loaded and having fulfilled both the previous conditions, the one-dimensional elastic plane stress wave propagation theory can be applied to the input bar-specimen-output bar system as it is widely reported in [6, 23].

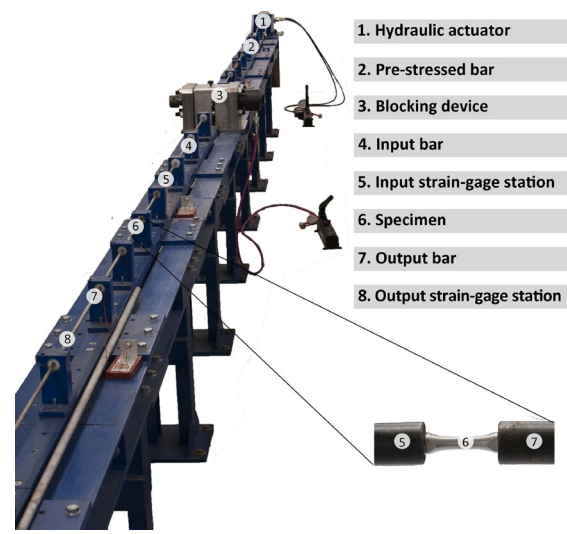

Fig. 3 JRC-Split Hopkinson Tensile Bar installed at the DynaMat Laboratory

Considering that A_0 is the cross-sectional area of output and input bars, A is the initial cross-sectional area of the specimen gauge length portion, L is the

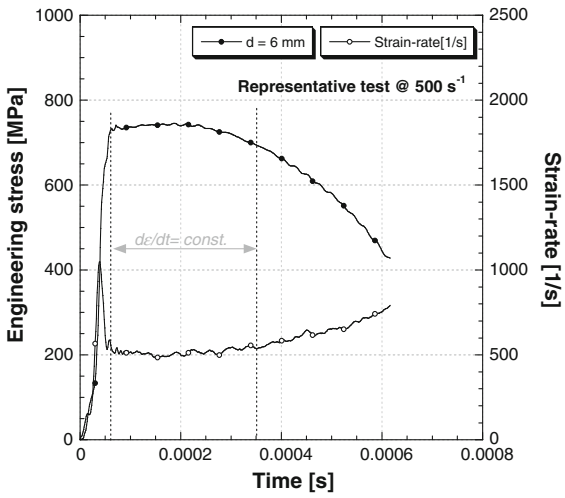

Fig. 4 Stress and strain-rate versus time of a test at 500 s^{-1}

gauge length of the specimen, t is the time, $C_0 = (E_0/\rho)^{1/2}$ is the bar elastic wave speed, where E_0 is the elastic modulus of the bars and ρ is the bar density, then the stress, the strain and the strain-rate in function on the time are evaluated with the following equations:

$$\sigma_E(t) = E_0 \frac{A_0}{A} \varepsilon_T(t), \tag{1}$$

$$\varepsilon_E(t) = -\frac{2C_0}{L} \int_0^t \varepsilon_R(t) \mathrm{d}t, \tag{2}$$

$$\dot{\varepsilon}(t) = -\frac{2C_0}{L} \varepsilon_R(t). \tag{3}$$

In Fig. 4 an example of both stress and strain rate in function of the time, evaluated using the previous Eqs. (2) and (3), are depicted. It is possible to observe that in the plastic zone the strain rate remains nearly constant.

4 Experimental results and discussion

The averaged tensile data at room temperature, such as the ultimate tensile stress and uniform strain, fracture stress and strain, yield stress as well as the reduction of area at fracture are summarised in Table 2. As a result of the high reproducibility of tests (Fig. 5), only three tests for each strain rate have been performed.

The comparison between static and dynamic tests at 500 s^{-1} for samples obtained from the three different diameters is reported in Fig. 6. As expected, in static conditions, the ultimate tensile stress increases while the fracture strain decreases with the decreasing of the diameter, due to the cold forming process that strengthen the material but with a reduction in ductility. By observing the dynamic results it is possible to point out that both the yield strength (f_y) and the ultimate tensile strength (f_t) present an increasing with the strain-rate. As a consequence, the strain rate has an important effect not only on the fracture strain, but also on the strength of the material. Another comparison is plotted in Fig. 7, where tests at 250, 500 and 1000 s^{-1} are reported for samples turned from the same bar (8 mm).

Because of the initial instability with upper and lower yield point a conventional yield stress was evaluated from the engineering stress versus strain curves as the intersection point of the lines fitted to the elastic and plastic regions of the curve.

In Fig. 8 the DIF of yield stress versus strain rate of several steels are depicted [13, 26–31]. From this figure can be observed how the steel with lower static yield stress has higher strain rate sensitiveness than those with higher static yield stress (indicated with filled symbols). The experimental results have been compared with the two existing relationships [8, 15, 16] able to provide DIF for both yield stress and ultimate tensile strength. Malvar [8], whose relationship was adopted in the

Table 2 Static and dynamic testing results

	$d = 6$ mm		$d = 8$ mm				$d = 10$ mm	
Strain rate (s^{-1})	10^{-4}	500	10^{-4}	250	500	1,000	10^{-4}	500
Yield stress (MPa)	586	728 ± 1	593	677 ± 3	717 ± 19	725 ± 18	555	677 ± 7
UTS (MPa)	652	748 ± 5	642	722 ± 10	744 ± 21	753 ± 20	579	695 ± 6
Uniform strain (%)	2.10	7.25 ± 1.2	2.51	6.35 ± 0.6	10.04 ± 2.0	6.41 ± 2.5	1.25	2.39 ± 1.3
Fracture stress (MPa)	400	409 ± 18	388	402 ± 17	395 ± 16	404 ± 12	331	334 ± 15
Fracture strain (%)	11.3	34.1 ± 2.3	12.3	28.7 ± 4.2	42.7 ± 6.4	34.8 ± 3.7	12.4	31.3 ± 1.4
Reduction of area (%)	64.50	66.50 ± 1.5	63.60	65.05 ± 1.7	66.87 ± 1.0	68.40 ± 0.7	68.20	69.03 ± 1.2

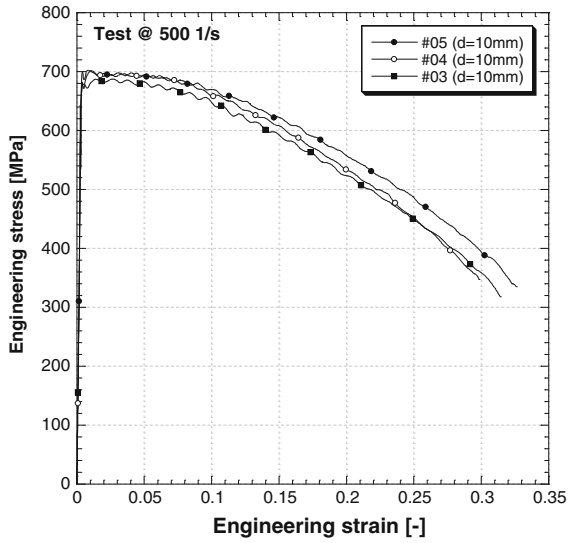

Fig. 5 Engineering stress versus strain of the samples obtained from $d = 10$ mm bars tested at 500 s^{-1}

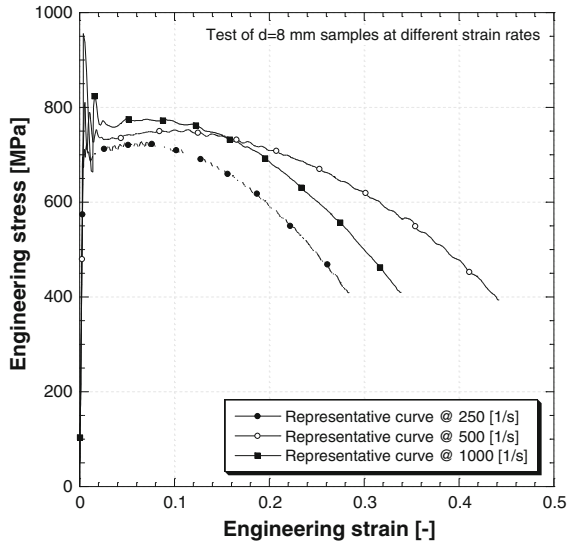

Fig. 7 Engineering stress versus strain at 250, 500 and 1000 s^{-1} for specimens turned from 8 mm bars

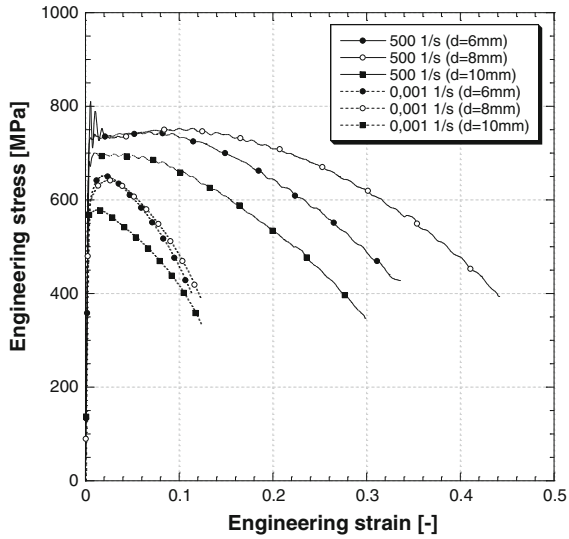

Fig. 6 Comparison between static and dynamic (500 s^{-1}) tensile tests

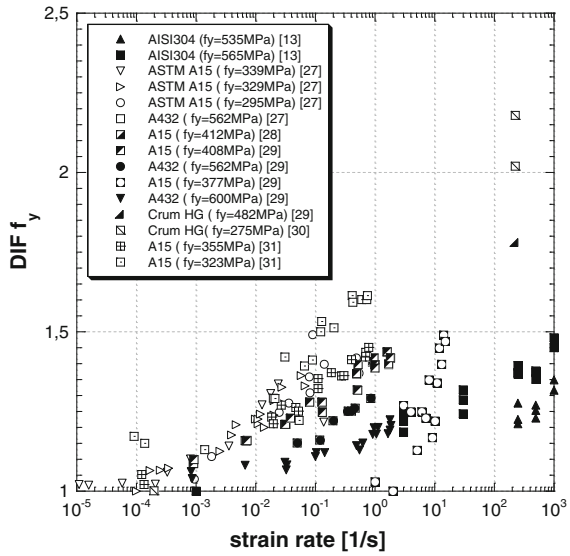

Fig. 8 DIF for yield stress versus strain rate

Model Code 2010 [16], proposed the following formulations, based on a review of the available studies in the strain rate sensitiveness of reinforcing steels:

$$\mathrm{DIF}(\alpha) = \left(\frac{\dot{\varepsilon}}{10^{-4}}\right)^{\alpha}, \tag{4}$$

$$\alpha(f_y) = 0.074 - 0.040 \cdot \frac{f_y}{414}, \tag{5}$$

$$\alpha(f_t) = 0.019 - 0.009 \cdot \frac{f_y}{414}. \tag{6}$$

These formulations, for yield stress and ultimate tensile strength, are valid only for strain rates ranging from 10^{-4} and 10 s^{-1} and for $290 < f_y < 710$ MPa.

The upper limit of 10 s^{-1} in [8] is due to the lack of data for higher strain rates. In [16] has been adopted a previous relationship in which the validity was

extended to 10^3 s^{-1}, but without any experimental results basis.

In [15], based on the regression analysis of past experimental results, several formulations for different steel types were presented, providing DIF for both ultimate tensile strength and yield stress. In case of cold drawn reinforcing steel, the formulations were:

$$\mathrm{DIF}(f_y) = \frac{f_{y,dyn}}{f_{y,static}} = 1 + \frac{6.0}{f_{y,static}} \cdot \ln\frac{\dot{\varepsilon}}{\dot{\varepsilon}_0}, \quad (7)$$

$$\mathrm{DIF}(f_t) = \frac{f_{t,dyn}}{f_{t,static}} = 1 + \frac{7.0}{f_{t,static}} \cdot \ln\frac{\dot{\varepsilon}}{\dot{\varepsilon}_0}, \quad (8)$$

where $\mathrm{DIF}(f_t)$ and $\mathrm{DIF}(f_y)$ are the ultimate tensile strength and yield stress DIF, respectively, $f_{y,static}$ and $f_{y,dyn}$ are the static and dynamic yield stress while $f_{t,static}$ and $f_{t,dyn}$ are the static and dynamic ultimate tensile strength, respectively, $\dot{\varepsilon}$ is the considered strain rate and $\dot{\varepsilon}_0$ is the quasi-static strain rate.

In Fig. 9 is shown a comparison between the obtained experimental data and the proposed formulations (4–8) referred to the data from the 8 mm bar.

As shown before also in this case it is possible to point out that the DIF of ultimate tensile strength is lower than DIF of yield stress. Furthermore, the values of DIF obtained by tests on specimens turned from bars lower diameter (6 mm) were more marked with respect to the ones from higher diameter (8 mm).

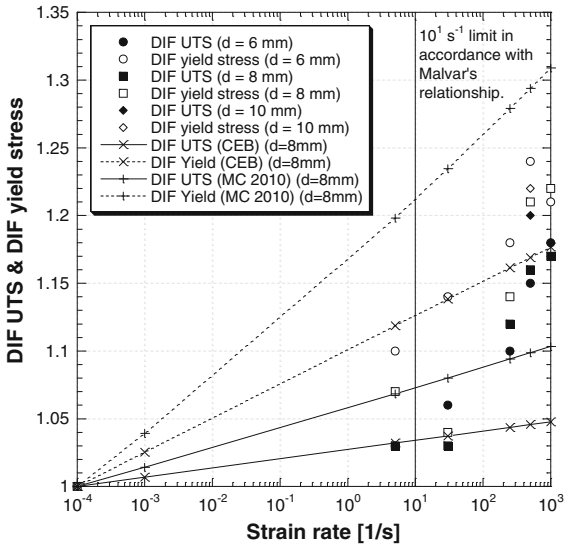

Fig. 9 Comparison between DIF results and the predictive formulation [8, 15, 16] versus strain rate

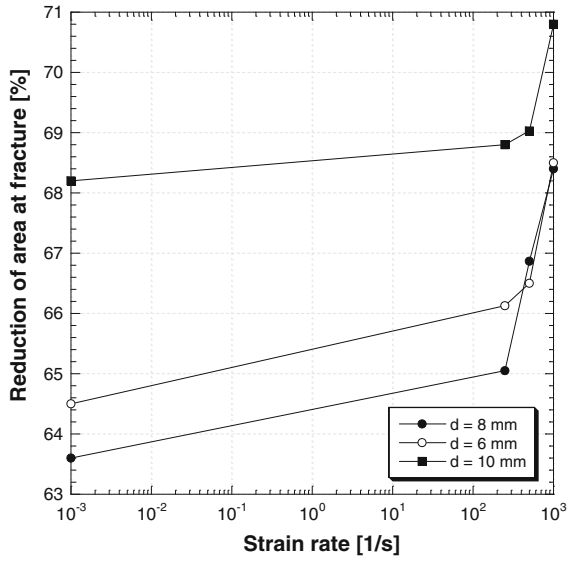

Fig. 10 Reduction of area at fracture in function of the strain rate

Considering that Malvar's relationships are valid only for strain rates range $10^{-4} \leq \dot{\varepsilon} \leq 10$ s^{-1} and for $290 < f_y < 710$ MPa and in addition no particular reference is reported for cold drawn steel, this equation clearly overestimates the experimental DIF obtained for yield stress, while it is quite acceptable for ultimate tensile strength DIF. On the contrary, the CEB bulletin [15] reports a specific relationship valid for cold working reinforcing steels, and even if it is valid only for strain rates up to 10 s^{-1}, conduct to a better approximation of our experimental data. In conclusion, for a better estimation of experimental data with strain rates higher than 10 s^{-1}, another equation should be reformulated.

The ductility can be also revealed by comparing the reduction of cross-sectional area in necked region observed after fracture of samples tested at different strain rates (Fig. 10). Samples turned from bars with higher diameter ($d = 10$ mm) show an higher ductility with respect to samples obtained from bars with lower diameter ($d = 6$ and 8 mm). In addition, a slight increase in ductility it is observed in samples from 10 mm bars as well as a remarkable increase in ductility it is noted in samples from bars with smaller diameters, which present a very similar behaviour.

Representative true stress versus true strain data regarding samples obtained from different bar diameters tested at 500 s^{-1}, were reported in Fig. 11.

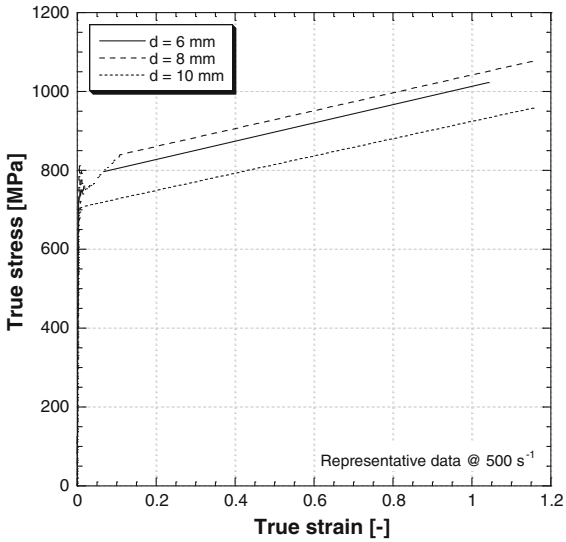

Fig. 11 True stress versus true strain at 500 s^{-1} of the materials from the bars having three diameter

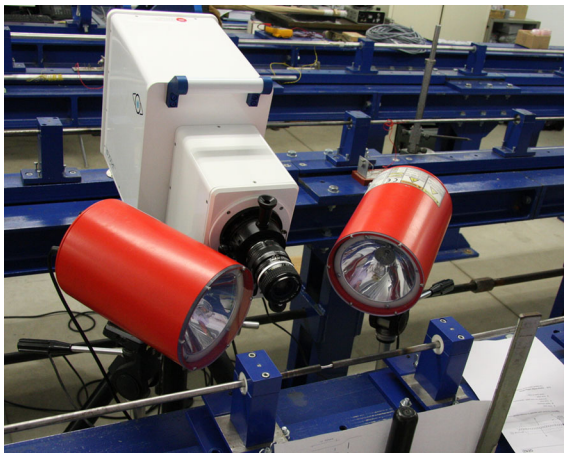

Fig. 12 Specialized Imaging Duplex Ultra Fast Framing Camera System used in this research

In order to analyse the failure behaviour of B500A steel, one test has been recorded by a Specialized Imaging Duplex Ultra Fast Framing Camera with a maximum speed up to 200 Mfps (Fig. 12), able to record up to eight images without compromising on shading or parallaxing with resolution 1,360 × 1,024.

In Fig. 13 the load versus time with the indication of photos made by the fast camera is shown. The failure's photo reveal the ability of the camera, set to take the picture every 5×10^{-5} s, to capture the necking process.

The true stress versus true strain curve is regarded as significant until the ultimate tensile stress (where the necking begins), is reached. After this point, stress localization and fracture propagation governs the flow curve, which is no more representative of homogeneous mechanical properties of the materials. In this case, beyond the point of ultimate strength in the engineering stress–strain curve, the one-dimensional true stress–strain curve should be reconstructed, by calculating the true stress and the true strain using the Bridgman formulae [32], which introduces the correction for the triaxial stress state. At fracture the Bridgman formulae can be written as follows:

$$\sigma_{\text{true,fracture}} = \frac{\sigma_{\text{eng,fracture}}}{\left(1+\frac{2R}{a}\right)\cdot \ln\left(1+\frac{a}{2R}\right)}, \tag{9}$$

$$\varepsilon_{\text{true,fracture}} = 2\cdot \ln\left(\frac{D_0}{2a}\right), \tag{10}$$

where a is the minimum radius at fracture cross-section, R is the meridional profile radius at fracture neck and D_0 is the initial diameter of the gauge length cross section.

For the complete construction of the true stress–strain curve during the necking deformation phase, a straight line is drawn between the ultimate tensile strength (uniform strain) point and the fracture point, the latter determined by application of Eqs. (9) and (10).

A more refined determination of the true stress versus true strain curve between the point of ultimate tensile strength and the point of fracture based on the fast recording has been performed [33]. At defined increasing deformations levels, an optical measurement of both the meridional radius at neck (R) and of the minimum radius at neck cross-section (a), has been carried out. Then, by using the Eq. (10), the true strain values for the defined deformation levels have been evaluated. Finally, using the couple of six load values and diameters, taken at the time of the six photos, it has been possible to evaluate the corresponding true stresses.

In Fig. 14 the results of the described measurement are shown, where it is possible to observe how the linear trend well describes the necking process in true stress versus true strain diagram. Subsequently it has been demonstrated the good approximation of the procedure which only exploits the Bridgman formulae and the information given by the engineering curve and by the measurement of the fracture geometry.

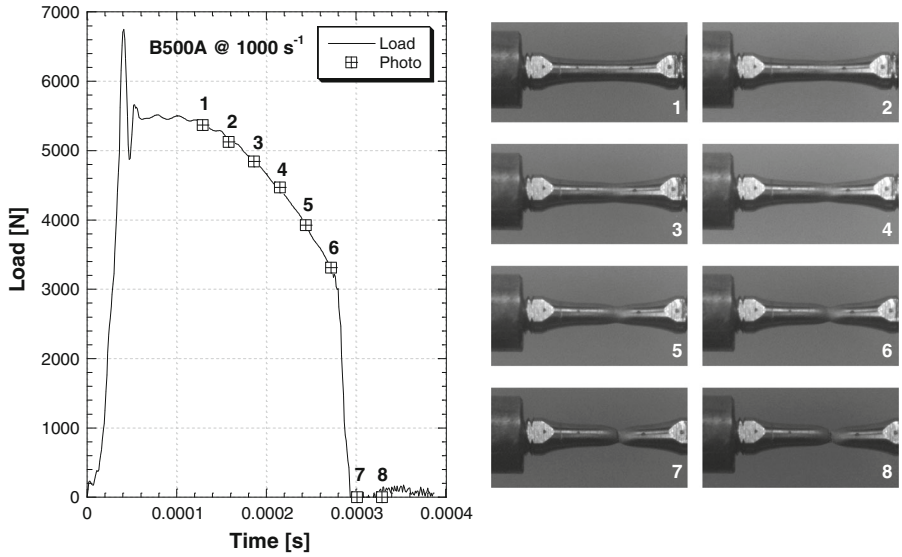

Fig. 13 Load in function of the time with the timeline of pictures taken with the fast camera

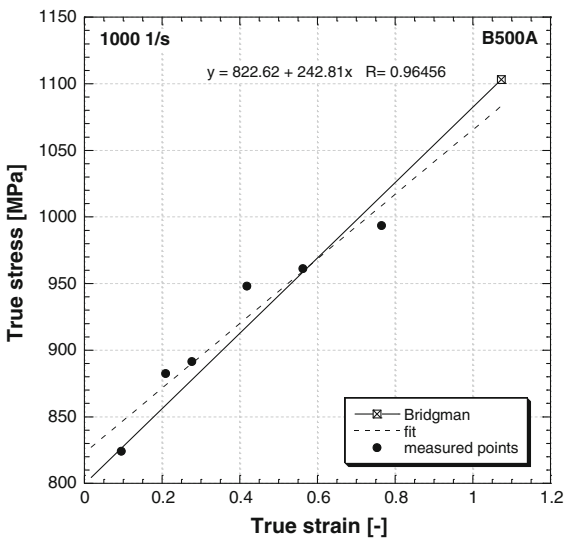

Fig. 14 Comparison between the true measured and calculated values

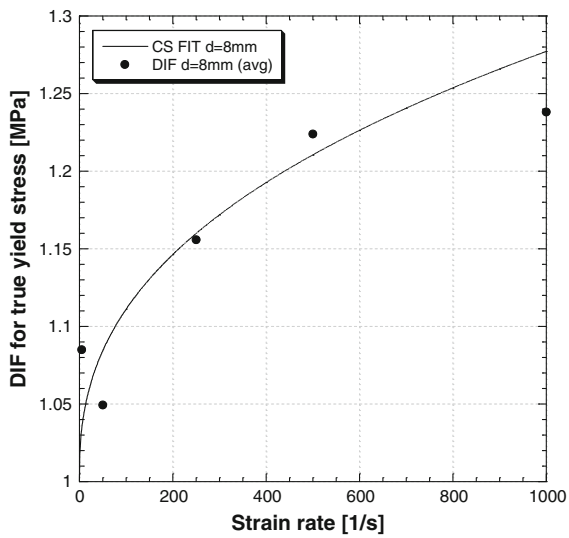

Fig. 15 Comparison between the experimental data and the Cowper–Symonds model for samples obtained from $d = 8$ mm bars

5 Calibration of material constitutive relationship

The strain rate sensitivity could be predicted by numerous constitutive equations available in literature. With these constitutive equations it is possible to predict the dynamic behaviour in function of the strain rate in order to assess a finite element analysis.

One of the common and widely used constitutive equation (11), is proposed by Cowper and Symonds [34]. This strain rate dependent elastic–plastic model is able to relate the dynamic stress with the strain rate by means of two constants D and q.

$$\frac{f_{\text{dyn}}}{f_{\text{stat}}} = 1 + \left(\frac{\dot{\varepsilon}}{D}\right)^{1/q}, \tag{11}$$

where f_{dyn} is the dynamic yield true stress, f_{stat} is the static yield true stress, $\dot{\varepsilon}$ is the strain rate, D and q are material parameters. An example of the goodness of this constitutive model is represented in Fig. 15, where a comparison between the experimental data

Table 3 Material parameters

Materials	Johnson–Cook				Cowper–Symonds	
	A (MPa)	B (MPa)	n (–)	c (–)	q (–)	D (–)
B500A ($d = 6$ mm)	588.9	535.6	0.4561	0.01599	4.4677	525,444
B500A ($d = 8$ mm)	595.6	687.5	0.5995	0.01803	2.5198	25,361
B500A ($d = 10$ mm)	558.4	289.4	0.4972	0.03207	1.6574	5,574

and the Cowper–Symonds model for samples obtained from $d = 8$ mm bars is reported. The obtained parameter for the three samples obtained from different diameters bare were reported in Table 3.

Another well-known constitutive equation (12) is proposed by Johnson and Cook [35], that is a widely used model able to describe the material strength in numerical simulation of dynamic event. Even if this model is based on three independent phenomena, the isotropic hardening, the strain rate hardening and the thermal softening, the influence of temperature will be considered in a future planned analysis.

$$\sigma = \left[A + B \cdot \left(\varepsilon_{\mathrm{p}}\right)^{n}\right] \cdot \left[1 + C \cdot \ln\left(\frac{\dot{\varepsilon}_{\mathrm{p}}}{\dot{\varepsilon}_{0}}\right)\right] \cdot \left[1 - \hat{T}^{m}\right], \tag{12}$$

where ε_{p} is the equivalent plastic strain, $\dot{\varepsilon}_{\mathrm{p}}$ is the strain rate in the test under consideration, $\dot{\varepsilon}_{0}$ is a reference strain rate, $\hat{T}$ is a dimensionless temperature, while the parameters that have to be determined from the experimental results are A, B, and n in order to take into account the strain-hardening, as well as C and m that represent the strain-rate sensitivity and the thermal softening, respectively.

The values of the above parameters are shown in Table 3.

6 Concluding remarks

The behaviour in tension at high strain rates of the commercial B500A grade high-strength reinforcing steel produced by cold forming process was herein investigated. The mechanical behaviour of the B500A strongly depends on the drawing machine as well as on the reduction factor of the diameter of original wire. As expected due to the cold forming process, the ultimate tensile stress increases while the fracture strain decreases with the decreasing of the diameter.

A significant effect on the strength of the material on both yield and tensile strength are obtained with the increase of the strain rate.

By analysing the data on the reduction of cross-sectional area in the necked region after fracture it is possible to point out that samples turned from bars with higher diameter present an higher ductility with respect to samples obtained from bars with lower diameters.

By means of a high speed framing camera a verification of the well-known Bridgman formulae has been performed. The obtained results shown how the linear trend well describes the necking process in true stress versus true strain plot.

Lastly, two of the common constitutive equation proposed by Cowper–Symonds and Johnson–Cook, and extensively used in many finite element computer analysis were taken into consideration. The material parameters were then evaluated from the experimental data.

These results have highlighted that increasing the strain rate will results in increases in strength capacity of the reinforcing bar as well as occurs for concrete both in tension and compression. The improved capacities of the materials are reflected in the axial and flexural capacity of the RC members. Concrete confinement is positively influenced by the presence of the transverse reinforcement with higher strength capacity. Some drawback must to be taken into account when the strain rate increases [36]. Due to the significant increases of the material strengths the formation of the plastic hinges may be delayed and their location could be difficult to define. Another undesirable effect consists in the possible shifting of the failure mode from ductile flexural failure to a brittle shear failure. Unfortunately very little is the knowledge about the shear behaviour at high strain rate about concrete, reinforcing bar and bond between them. Future researches will be addressed to providing reliable data on the aforementioned problems.

Acknowledgments A special acknowledgement goes to Mr. Wai Chan and Mr. Peter Berkenberg from "Specialised Imaging" for their precious collaboration in the execution of high speed measurements.

References

1. Ngo T, Mendis P, Gupta A, Ramsay J (2007) Blast loading and blast effects on structures—an overview. EJSE Special Issue: Loading on Structures 76–91
2. Asprone D, Cadoni E, Prota A (2009) Experimental analysis on tensile dynamic behaviour of existing concrete under high strain rates. ACI Struct J 106:106–113
3. Asprone D, Cadoni E, Prota A (2009) Tensile high strain-rate behavior of reinforcing steel from an existing bridge. ACI Struct J 106:523–529
4. Bassim MA, Panic N (1999) High strain rate effects on the strain of alloy steels. J Mater Process Technol 92–93:481–485
5. Ogawa K (1985) Mechanical behaviour of metals under tension–compression loading at high strain rates. Int J Plast 1:347–358
6. Cadoni E, Dotta M, Forni D, Tesio N, Albertini C (2013) Mechanical behaviour of quenched and self-tempered reinforcing steel in tension under high strain rate. Mater Des 49:657–666
7. Dowling AR, Harding J (1967) Tensile properties of mild steel under high strain rates. In: Proceedings of the 1st HERF conference, University of Denver, Colorado, 1967
8. Malvar LJ (1998) Review of static and dynamic properties of steel reinforcing bars. ACI Mater J 95:609–616
9. Mainstone RJ (1975) "Properties of materials at high rates of straining or loading", part 4, state-of-the-art report on impact loading of structures. Mater Struct 8:102–116
10. Norris GH, Hansen RJ, Holly MJ, Biggs JM, Namyet S, Minami JK (1959) Structural design for dynamic loads. McGraw-Hill, New York
11. Uenishi A, Teodosiu A (2004) Constitutive modelling of the high strain-rate behaviour of 7 interstitial-free steel. Int J Plast 20:915–936
12. Lee WS, Liu CY (2006) The effect of temperature and strain-rate on the dynamic flow behaviour of different steels. Mater Sci Eng A 426(1–2):101–113
13. Cadoni E, Fenu L, Forni D (2012) Strain rate behaviour in tension of austenitic stainless steel used for reinforcing bars. Constr Build Mater 35:399–407
14. Cadoni E, Dotta M, Forni D, Tesio N (2011) Dynamic behaviour of reinforcing steel bars in tension. Appl Mech Mater 82:86–91
15. CEB (1998) Concrete structures under impact and impulsive loadings. Bull Inf 187:1–183
16. FIB-International Federation for Structural Concrete, Model Code 2010, Bulletin number 66 (2012)
17. Abu-Lebdeh T, Hamoush S, Choi W, Al Nasra M (2011) High rate-dependent interaction diagrams for reinforced concrete columns. Am J Eng Appl Sci 4(1):1–9
18. Player JR, Morton EC, Thompson AG, Villaescusa E Testing and analysis of steel wire mesh for mining applications of rock surface support. In: 6th International symposium on ground support in mining and civil engineering constructions
19. Eurocode 2: EN 1992-1-1:2004 (2004) Design of concrete structures. General rules and rules for buildings
20. Swiss Norm, SN 505 262. Concrete structures, SIA262: 2013
21. French Norm, NF A35-080, Aciers pour béton armé—Aciers soudables (2010)
22. Cadoni E, Dotta M, Forni D, Spaetig P (2011) Strain-rate behavior in tension of the tempered martensitic reduced activation steel Eurofer97. J Nucl Mater 414(3):360–366
23. Cadoni E (2010) Dynamic characterization of orthogneiss rock subjected to intermediate and high strain rate in tension. Rock Mech Rock Eng 43:667–676
24. Asprone D, Cadoni E, Prota A, Manfredi G (2009) Strain-rate sensitivity of a pultruded E-glass/polyester composite. ASCE J Compos Constr 13(6):558–564
25. Albertini C, Montagnani M (1974) Testing techniques based on the split Hopkinson bar. Inst Phys Conf Ser 21:22–32
26. Keenan WA, Feldman A (1960) The yield strength of intermediate grade reinforcing bars under rapid loading. Behavior and Design of Deep Structural Members, Part 6, Technical Report AFSWC-TR-59-72, Research Directorate, Air Force Special Weapons Center, Kirtland Air Force Base, New Mexico, March 1960 (also: University of Illinois, Structural Research Series 197)
27. Seabold J (1970) Dynamic shear strength of reinforced concrete beams—Part III, Technical Report R695. Naval Civil Engineering Laboratory, Port Hueneme
28. Cowell WL (1965) Dynamic tests of concrete reinforcing steels, Technical Report R394. Naval Civil Engineering Laboratory, Port Hueneme
29. Keenan W, Tancreto J, Meyers G, Johnson F, Hopkins J, Nickerson H, Armstrong W (1983) NCEL products supporting DOD revision of NAVFAC P-397, Technical Memorandum 51-83-19 (previously 2591TM). Naval Civil Engineering Laboratory, Port Hueneme
30. Crum RG (1959) Tensile impact tests for concrete reinforcing steels. ACI J Proc 56(1):59–61
31. Wood DS (1956) Rapid loading tests on three grades of reinforcing steel, Contract Report R-56-5 under Contract N0y-90922. Naval Civil Engineering Laboratory, Port Hueneme
32. Bridgman PW (1952) Studies in large plastic flow and fracture. McGraw-Hill, New York
33. Cadoni E, Bragov AM, Dotta M, Forni D, Konstantinov A, Lomunov A, Ripamonti A (2011) Mechanical characterization of steel for fastening in a wide range of strain rate. Eng Trans 59(2):101–117
34. Cowper GR, Symonds PS (1957) Strain hardening and strain rate effect in the impact loading of cantilever beams. Brown University, Division of Applied Mathematics report number 28
35. Johnson GJ, Cook WH (1985) Fracture characteristics of three metals subjected to various strains, strain rates, temperature and pressure. Eng Fract Mech 21:31–48
36. Fu HC, Seckin M, Erki MA (1991) Review of effects of loading rate on reinforced concrete. ASCE J Struct Eng 117(12):3660–3679